DOI: 10.1002/ejoc.200700466

One-Pot Synthesis of Core-Modified Rubyrin, Octaphyrin, and Dodecaphyrin: Characterization and Nonlinear Optical Properties

Rajeev Kumar,[a] Rajneesh Misra,[a] Tavarekere K. Chandrashekar,*[a,b] Amit Nag,[a] Debabrata Goswami,[a] Eringathodi Suresh,[c] and Cherumuttathu H. Suresh[b]

Keywords: Expanded porphyrin / Conjugation / Porphyrinoids / Anion binding / TPA cross section

Modified 26π rubyrin, 36π octaphyrin, and 54π dodecaphyrin systems have been synthesized in moderately good yields through acid-catalyzed condensations of terthiophene diols and tripyrranes. The product distributions are decided both by the acid catalyst concentration and by the nature of the *meso* substituents. For example, a new isomer of [26]hexaphyrin(1.1.1.1.0.0) (rubyrin) was obtained with 0.3 equiv. of *p*-toluenesulfonic acid, when the *meso* substituent was mesityl in at least one of the precursors. A change of the mesityl substituent for a *p*-methoxy substituent in terthiophene diol resulted in the formation of a [3+3+3+3] condensation product – [54]dodecaphyrin(1.1.1.1.0.0.1.1.1.1.0.0) – in addition to the expected rubyrin. Furthermore, an increase in the acid concentration to 0.6 equiv. resulted in the formation of a new [36]octaphyrin(1.1.1.1.1.1.0.0), in addition to the rubyrin and dodecaphyrin. A single-crystal X-ray analysis of octaphyrin represents the first example of a planar conformation of an octaphyrin with six *meso* links. In rubyrin **19**, one thiophene ring, opposite to the terthiophene subunit, is inverted, while in octaphyrin **30** one pyrrole ring and two thiophene rings are inverted. The various conformational possibilities tested for the unsubstituted dodecaphyrin **28**, at semiempirical level, suggest that the most stable conformation is a figure-eight. The final geometry optimization of figure-eight dodecaphyrin was done at the B3LYP/6-31G* level of DFT. Octaphyrins and dodecaphyrins bind trifluoroacetate anion effectively in their diprotonated forms, the binding constants (*K*) being 638 M^{-1} for dodecaphyrin **28**, and 415 M^{-1} for octaphyrin **30**. Electrochemical data reveal HOMO destabilization with increasing π electron conjugation, consistently with the large red shifts of the absorption bands. Preliminary studies on the use of these expanded porphyrins as third-order NLO materials were followed by measurements of their two-photon absorption (TPA) cross-sections [$\sigma^{(2)}$]. The $\sigma^{(2)}$ values increase upon going from the 26π rubyrins to the 54π dodecaphyrins, confirming our earlier observation that increases in π-conjugated electrons increase the TPA values.

Introduction

Research into syntheses of new aromatic core-modified expanded porphyrins, in which one or more pyrrole rings are replaced by other heterocyclic rings such as thiophene, furan, or selenophene, continue to attract the attention of chemists, due to their diverse applications as, for example, anion receptors,[1] transition or lanthanoid ion chelates,[2] sensitizers for photodynamic therapy,[3] and contrast agents in magnetic resonance imaging (MRI).[4] These fascinating properties have encouraged synthetic efforts towards a variety of expanded porphyrins differing in ring size, ring connectivity, peripheral substituents, and core modification. Such modification not only alters the electronic structure, but also induces structural diversity in the form of ring inversions in the resulting macrocycles. Apart from a host of diverse applications, they can also be used as a tool for accessing currently unknown higher aromatic systems. In recent years, organic molecules capable of exhibiting large nonlinear optical susceptibilities have attracted the attention of chemists because of their diverse technological applications in three-dimensional microfabrication, optical limiting, and data storage.[5] The presence of extended π electron delocalization is the key element in the design of organic molecules for nonlinear optical applications. Thus, the design and synthesis of new molecules with large macroscopic optical nonlinearities represent an active research field in modern chemistry and materials science. Porphyrins and expanded porphyrins are one class of organic molecules suitable for nonlinear optical applications. These systems are popular because of the π electron delocalization required for electronic communication, their high thermal stabilities, and the versatile modifications of the structure possible in the basic framework of the macrocycle skeleton. Recent work from this laboratory has shown that an increase in the number of π electrons in the conjugated path-

[a] Department of Chemistry, Indian Institute of Technology, Kanpur 208016, India
E-mail: tkc@iitk.ac.in
[b] Regional Research Laboratory, Trivandrum, Kerala 695019, India
Fax: +91-471-2491712
[c] E. Suresh, Central Salt & Marine Chemicals Research Institute, Bhavnagar, Gujarat 364002, India

Supporting information for this article is available on the WWW under http://www.eurjoc.org or from the author.

way enhances the two-photon absorption cross-section [$\sigma^{(2)}$] values considerably.[5]

Rubyrins such as **1** are a class of hexaphyrin in which six pyrrole rings are linked to each other through four *meso* bridges. Unlike **1**, the *meso* aryl rubyrins **3**–**6**, in which the pyrrole rings are unsubstituted, exhibit structural diversity.[6] Depending upon the nature of the link and the heteroatom present in the cavity, two structural congeners are known in the literature:[7,8] normal as in **5** and inverted as in **2**, **3**, **4**, and **6**. Sessler and co-workers reported the synthesis of **2** by an acid-catalyzed condensation reaction of diphenyltripyrrane with diformylhexamethylterpyrrole, in which one precursor was a β-substituted pyrrole derivative and the other a *meso* phenyl-substituted derivative.[8] Therefore, in **2**, the pyrrole ring adjacent to the *meso* phenyl substituents is inverted. These studies clearly reveal that the structures of the rubyrins are dependent upon the *meso* substituents present in the precursors before the condensation or coupling reaction. We have found that *meso* substituents present on the precursors and the acid catalyst concentration both play crucial roles in syntheses of expanded porphyrins. In this paper we wish to report on the synthesis, characterization, and properties of new isomers of [26]hexaphyrin(1.1.1.1.0.0), [36]octaphyrin(1.1.1.1.1.1.0.0), and [54]-dodecaphyrin(1.1.1.1.0.0.1.1.1.1.0.0). The variations in the products formed have been investigated in detail through variation of the *meso* aryl substituents and acid catalyst concentrations. The two-photon absorption cross-section [$\sigma^{(2)}$] values measured by the open aperture Z-scan method depend on: i) the effect of π conjugation, ii) the effect of core heteroatoms (S vs. Se), and iii) the effect of *meso* aryl substituents. The $\sigma^{(2)}$ values increase with increasing π electron conjugation (i.e., from 26π to the 54π systems).

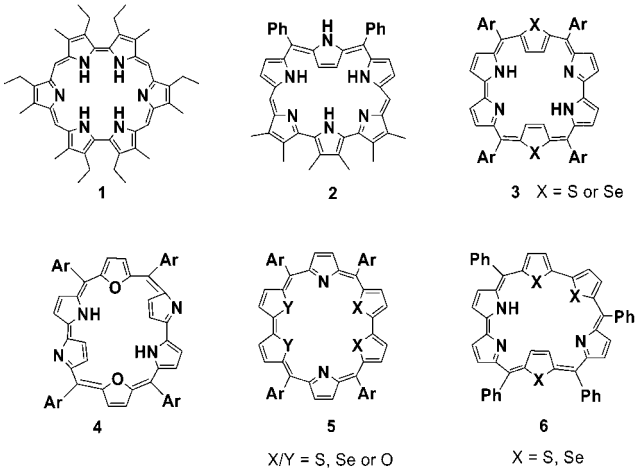

Results and Discussion

Syntheses

In these syntheses an efficient approach involving [3 + 3] acid-catalyzed condensations of terthiophene diols[9] **7**–**10** and tripyrranes **11**–**14** was applied (Scheme 1). Mixtures of the appropriate diol and tripyrrane were stirred in the presence of *p*-toluenesulfonic acid (PTSA) in dry CH_2Cl_2 in the dark at room temperature. Stirring (90 min) under nitrogen, followed by chloranil oxidation in air and purification by column (alumina, grade III) chromatography, gave the expected rubyrins **15**–**24**. We found that product distributions and the natures of the expanded porphyrins formed in the reactions depended on the *meso* substituents present on the precursors and the concentrations of the acid catalyst. To understand this aspect further, we looked into this condensation reaction using different *meso* substituents on the precursors (i.e., the diols and the tripyrranes), and varying the acid concentrations. New isomers of rubyrins **15**–**24** could be obtained in good yields (20–25%) by using 0.3 equiv. PTSA, when the *meso* substituent in at least one of the precursors was a mesityl group. The expected rubyrins were not formed when the *meso* substituents were phenyl or tolyl in both the precursors, indicating the necessity of the bulkier group in at least one of the precursors, while keeping the acid concentration the same and changing the mesityl substituents for a *p*-methoxy substituent in the terthiophene diol resulted in the formation of [3 + 3 + 3 + 3] condensation products – [54]dodecaphyrins **28** and **29** – in 6–8% yields in addition to the expected rubyrins **26** and **27**, in 10–15% yields[10b] (Scheme 2). Furthermore, when the acid concen-

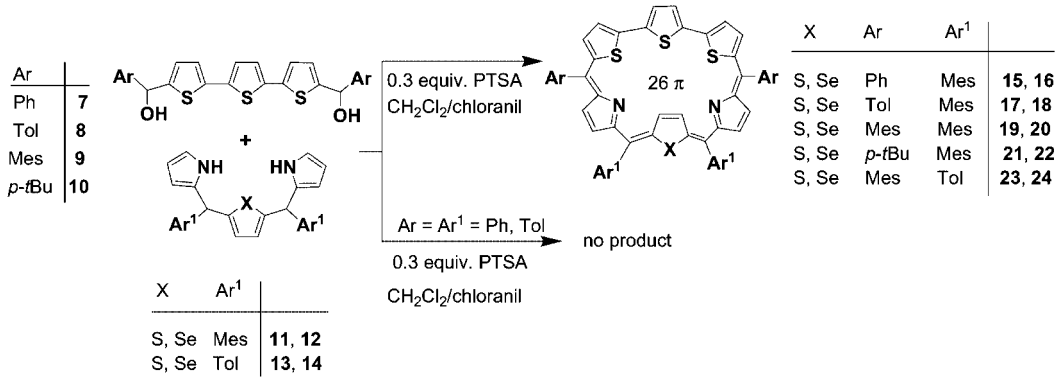

Scheme 1. Synthesis of rubyrins.

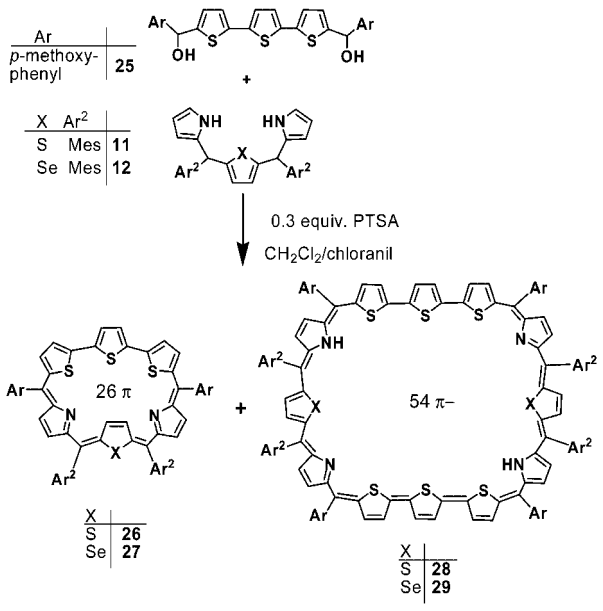

Scheme 2. Synthesis of rubyrins and dodecaphyrins.

tration was increased to 0.6 equiv., formation of [36]octaphyrins **30** and **31** in 10–12% yields was observed, in addition to the [26]rubyrins **26** and **27** in 10–12% yields and the [54]dodecaphyrins **28** and **29** in 5–6% yields (Scheme 3). It is well known that tripyrranes and tetrapyrranes undergo acidolysis in the presence of acid and that the extent of acidolysis depends on the concentration of acid in the reaction mixture.[9,11] Acidolysis of **11** and **12** has already been reported.[9] It has been reported that in the reaction of tripyrranes **11** or **12**, with 0.3 equiv. TFA as catalyst, 30π heptaphyrins were also formed in addition to the expected 26π rubyrins.[9,11d] The formation of trace amounts of porphyrins and 22π sapphyrins was also noticed.[11e] The formation of octaphyrins **30** and **31** can be explained by considering the fragmentation of tripyrranes **11** or **12** and the recombination of the fragmented products with the diol **25**. Spectrophotometric and TLC analysis of the reaction mixture provides satisfactory evidence for the fragmentation of tripyrranes **11** and **12**, as reported earlier from our laboratory.[12] The formation of a [36]octaphyrin was also observed with a diol containing other *meso* substituents and use of 0.6 equiv. PTSA, but the yield was very low and further characterization of this compound was hampered. Increasing the acid concentration to 1 and 2 equiv. did not change the yield of octaphyrins but reduced the yields of rubyrins and dodecaphyrins to 2%. All compounds were found to be stable as free bases in the solid state and in solution. It is important to note here that the formation of a twelve-member macrocycle (i.e., dodecaphyrin) was achieved only when the *meso* aryl group in the terthiophene diol was *p*-methoxy. The exact reason for the formation of this compound only with the *p*-methoxy group is not yet established.

All the compounds reported here were characterized by FAB-MS, UV/Vis, ^{1}H (and wherever possible 2D) NMR spectroscopy, and single-crystal X-ray analysis. For example, the FAB mass spectrum of rubyrin **19** exhibited its parent ion peak at *m*/*z* 981 $[M + H]^+$. The corresponding selena derivative **20** exhibited the corresponding peak at *m*/*z* 1029 $[M + H]^+$. Similarly, octaphyrins **30** and **31** exhibited parent ion peaks at *m*/*z* 1365 $[M]^+$ and 1461 $[M]^+$, respectively, and dodecaphyrins **28** and **29** exhibited their parent ion peaks at *m*/*z* 1916 $[M + 2 H]^+$ and 2012 $[M + 2 H]^+$, respectively, confirming the proposed compositions.

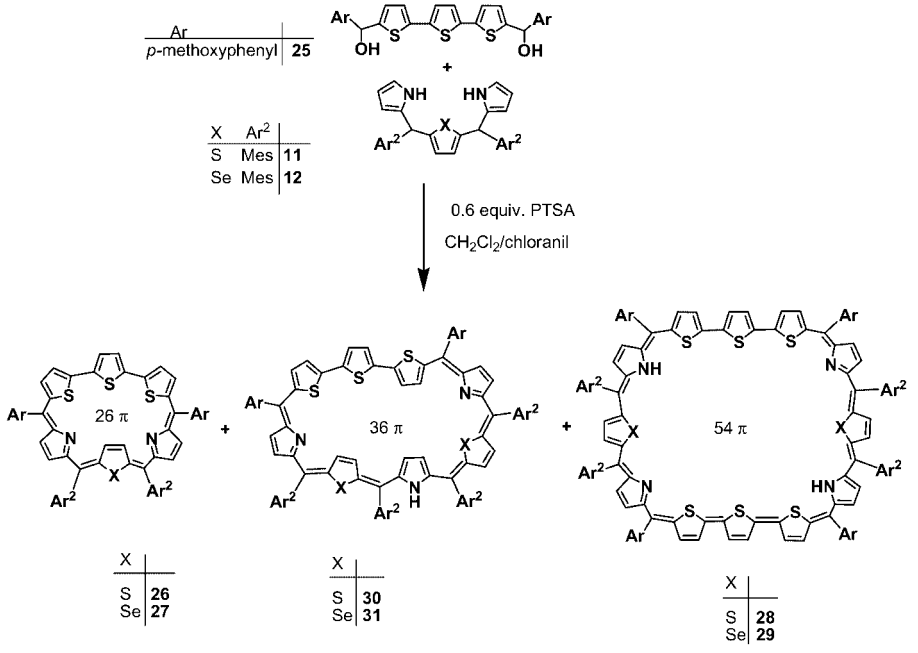

Scheme 3. Synthesis of rubyrins, octaphyrins, and dodecaphyrins.

^{1}H NMR Spectroscopy

A detailed analysis of the ^{1}H and 2D NMR spectra of **15**–**27** confirms the proposed solution structures. Both free base and diprotonated forms of rubyrin exhibit well resolved peaks in their ^{1}H NMR spectra at room temperature. A typical ^{1}H NMR spectrum observed for the free base of rubyrin **19** is shown in Figure 1, and the corresponding assignments, based on ^{1}H-^{1}H COSY correlations, are marked in the spectrum (see electronic supporting information). There are four sets of doublets between 7.62 and 9.61 ppm, integrating to two protons each, which are assigned to the four magnetically distinct β-CH protons. A singlet at δ = 9.70 ppm is ascribed to the β-CH protons of the central thiophene ring of the terthiophene unit, and two singlets at δ = 7.26 and 7.21 ppm are ascribed to the phenyl CH protons of two magnetically distinct mesityl rings. As anticipated, the thiophene ring opposite to the terthiophene unit is inverted both in the free base and in the protonated form (see Figure 1 and electronic supporting information).[10a] A similar ring inversion pattern was observed by Sessler and co-workers for an all-aza analogue of this rubyrin.[8] The single-crystal X-ray structure of TFA-bound rubyrin **19** has been given in a preliminary communication[10b] (CCDC-612135). In the free base form, the inner CH protons of the inverted thiophene ring are not seen even at 203 K, suggesting a rapid rotation of the ring, but after protonation with TFA the inner β-CH protons resonate as a sharp singlet at –3.64 ppm while the inner NH protons resonate as a broad singlet at –3.21 ppm (see supporting information). These data indicate a diatropic ring current for **19**.

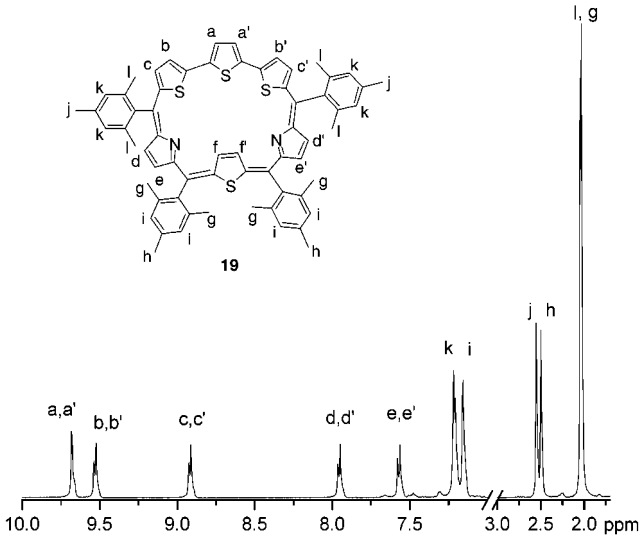

Figure 1. ^{1}H NMR spectrum of **19** in $CDCl_3$ at room temperature.

Octaphyrins **30** and **31** also exhibit well resolved peaks in their ^{1}H NMR spectra at room temperature. Specifically, the ^{1}H NMR spectrum of **30** measured in $CDCl_3$ shows twelve sets of doublets, integrating to one proton each, and two sets of triplets, integrating to two protons each, between 5.29 and 12.73 ppm, which are assigned to the sixteen magnetically distinct β-CH protons. The ^{1}H NMR spectrum observed for the free base form of **30** (Figure 2) suggests that **30** possesses a very low symmetry. Overall, three ring inversions could be observed. One of the terminal thiophene rings of the terthiophene subunit is inverted, as is another thiophene ring of the tripyrrane subunit. One pyrrole unit is also inverted, with NH pointing outside of the macrocycle. Four singlets observed at 6.78, 6.68, 6.52, and 6.47 ppm, integrating to two protons each, which were assigned to phenyl CH protons (p, m, o, n) of four mesityl rings and four doublets observed at 7.17, 7.10, 6.82, and 6.80 ppm, integrating to two protons each, were assigned to phenyl CH protons (l, j, k, i) of two aryl rings containing methoxy groups. The broad singlet at δ = 5.26 ppm is assigned to the pyrrole NH proton (q), and this NH proton shows correlation with β-CH protons e and e′ in the ^{1}H-^{1}H COSY spectrum. The peak at δ = 3.80 ppm was assigned to six methoxy protons, whereas the peaks in the 2.21 to 1.87 ppm region were assigned to the methyl protons of the *meso*-mesityl substituents. The corresponding assignments based on ^{1}H-^{1}H COSY correlations are marked in the spectrum (see electronic supporting information). Further findings are that, in octaphyrin **30**, the inverted NH proton resonates at δ = 5.26 ppm and not in the deshielded region and that upon D_2O exchange the signal is diminished (see supporting information). In addition, no peak was observed in the shielded region (expected for inner NH protons for a aromatic system) upon protonation with TFA, suggesting

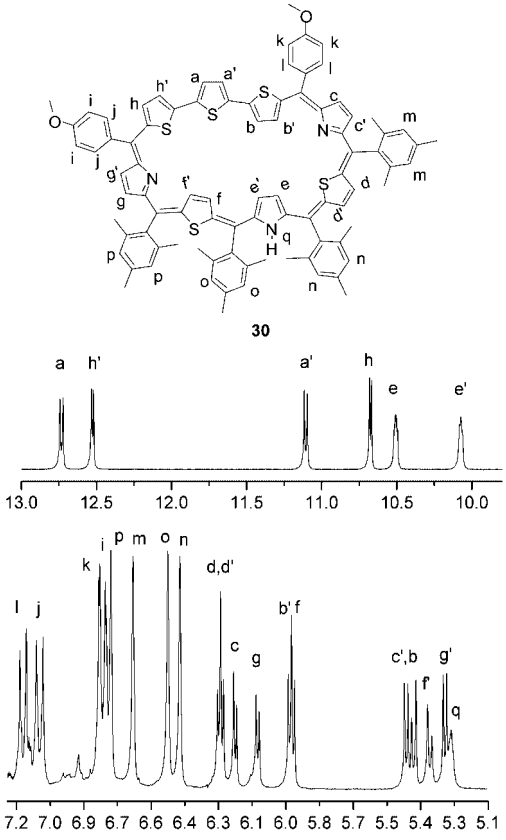

Figure 2. ^{1}H NMR spectrum of **30** in $CDCl_3$ at room temperature.

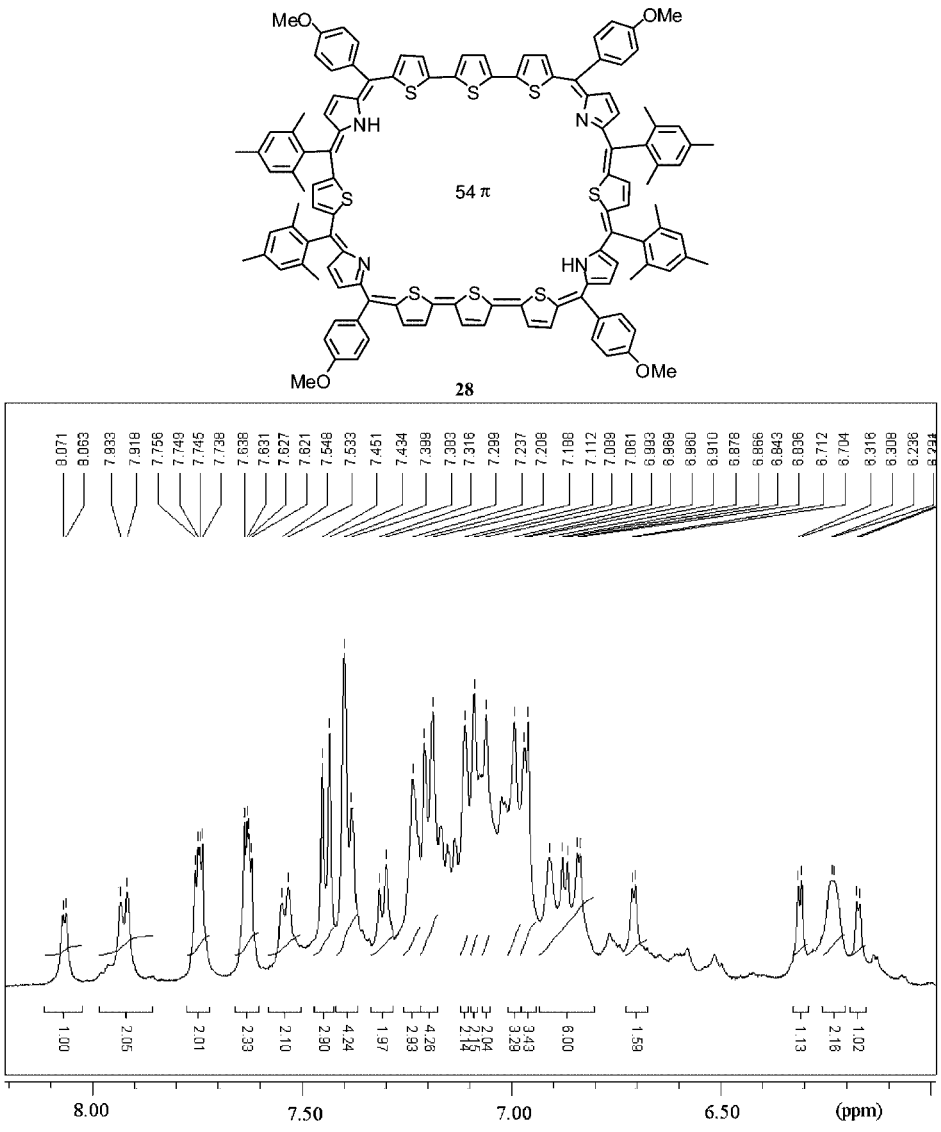

Figure 3. ^{1}H NMR spectrum of **28** in CD_2Cl_2 at 213 K.

the absence of a diatropic ring current, so the above octaphyrin is nonaromatic, as would be expected for 36π electrons in conjugation (4*n* system).

The ^{1}H NMR spectra of **28** and **29** were not well resolved at room temperature; however fairly-well resolved spectra were obtained in CD_2Cl_2 upon lowering the temperature to 213 K for **28** and **29**, in strong support of the well known fact that larger macrocycles exhibit conformational flexibility. Hence, at room temperature, no well resolved peaks could be obtained. At 213 K, however, the ^{1}H NMR spectrum of **28** in CD_2Cl_2 was well resolved (Figure 3). The peaks in the 6.0 to 8.2 ppm region are assigned to the phenyl protons and β-CH protons of the heterocyclic units, the peak at 3.9 ppm is assigned to the methoxy protons, whereas the peaks in the 1.2 to 2.4 ppm region are assigned to the methyl protons of the *meso* mesityl substituents. The correlations in the ^{1}H-^{1}H COSY spectra for **28** and **29** lacked clarity and hence the signals for the respective β-CH protons of the heterocyclic units could not be assigned.

Spectral Characterization

The electronic absorption spectrum of the free base form of rubyrin **19** exhibited a sharp Soret-like band at 527 nm ($\varepsilon = 1.90 \times 10^5$ M^{-1} cm^{-1}) and multiple Q-bands in the 600 to 730 nm region (Figure 4). Octaphyrin **30** exhibited a Soret-like band at 525 nm ($\varepsilon = 1.13 \times 10^5$ M^{-1} cm^{-1}) and one Q-band at 613 nm (Figure 5), while the dodecaphyrin **28** exhibited a Soret-like band at 604 nm ($\varepsilon = 1.16 \times 10^5$ M^{-1} cm^{-1}) and one Q-band at 744 nm (Figure 6). These data confirm the porphyrinoid natures of the macrocycles. Protonation in each case results in further red shifts of the Soret band and the Q-bands. For example, protonation of **19** upon addition of an excess of TFA in CH_2Cl_2 led to a red shift, splitting, and intensification of the Soret-like band to 557 nm ($\varepsilon = 2.62 \times 10^5$ M^{-1} cm^{-1}) and 606 nm ($\varepsilon = 1.61 \times 10^5$ M^{-1} cm^{-1}). The absorption bands of these rubyrins are found to be approximately 25 to 50 nm red-shifted relative to the all-aza analogues,[8] due to the substi-

tution of the heteroatoms in the macrocycle cores. A 85 nm shift of the Soret band on going from **15** to **29** is in line with the extension of π-conjugation from a 26π system to a 54π system. Protonation of **30** led to red shift in the Soret-like band to 622 nm ($\varepsilon = 1.52 \times 10^5$ M^{-1}cm^{-1}), and protonation of **28** led to a red shift in the Soret-like band to 710 nm ($\varepsilon = 1.82 \times 10^5$ M^{-1}cm^{-1}). Similar red shifts are observed in the Q-band region. Octaphyrins **30** and **31** and dodecaphyrins **28** and **29** bind with trifluoroacetate anion in their diprotonated forms. A careful TFA titration was performed to calculate the binding constant. Diprotonated octaphyrin **30**·2H$^+$ was characterized by the presence of two distinct bands at 622 and 702 nm. On further addition of TFA, the absorption maximum at 622 nm gradually decreased in intensity and the absorption maximum at 702 nm gradually increased (Figure 5). The diprotonated dodecaphyrin **28**·2H$^+$ was characterized by the presence of three bands at 710 nm, 842 nm, and 965 nm. On further addition of TFA, the absorption maximum at 710 nm underwent a red shift of 14 nm and the intensity of this band and of that at 842 nm gradually increased (Figure 6). The presence of isosbestic points in Figures 5 and 6 indicates the equilibrium between the free diprotonated species and the anion-bound complex, which indicates the strong TFA binding with the macrocycle. Higher binding constants were observed for the dodecaphyrins **28** [(*K*); 638 M^{-1}] and **29** [(*K*); 605 M^{-1}] than for the octaphyrins **30** [(*K*); 415 M^{-1}] and **31** [(*K*); 390 M^{-1}]. Recently, we have reported the solid-state X-ray structure of [34]octaphyrin binding with two TFA anions, one above and one below the macrocycle plane, the anions held by weak hydrogen bonding involving N–H···O, C–H···O, and C–H···F interactions.[13]

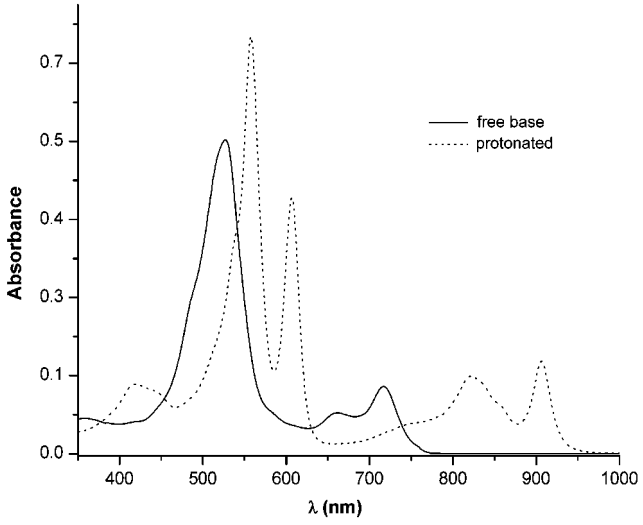

Figure 4. Electronic absorption spectra of **19** (−) (2.63×10^{-6} M) and its dication in CH_2Cl_2. The dication was generated by careful addition of TFA.

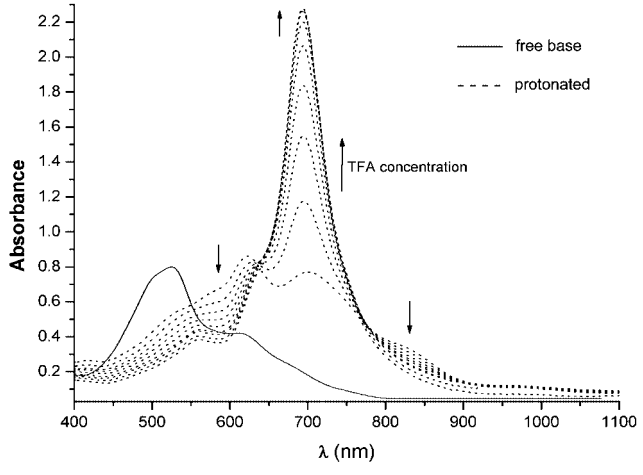

Figure 5. Electronic absorption spectra of **30** (−) (7.08×10^{-6} M) and UV/Vis response of **30** to the addition of TFA in CH_2Cl_2. The dication was generated by careful addition of TFA.

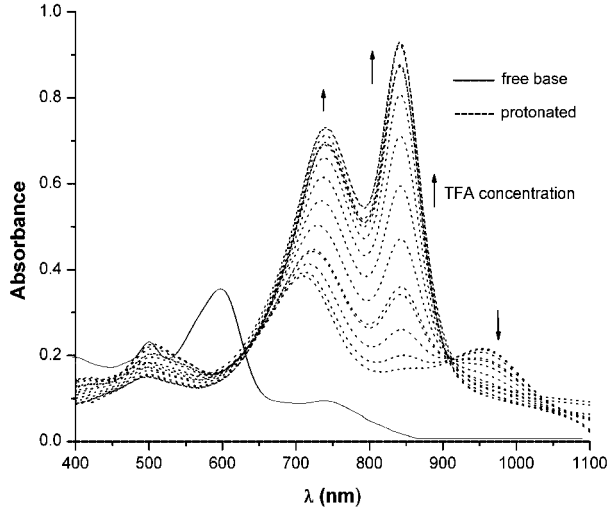

Figure 6. Electronic absorption spectra of **28** (−) (3.01×10^{-6} M) and UV/Vis response of **28** to the addition of TFA in CH_2Cl_2. The dication was generated by careful addition of TFA.

Structural Characterization

The proposed octaphyrin structure was further confirmed by solving the single-crystal X-ray structure for **30** (CCDC-632328), which shows a nearly planar conformation. It is known from the literature that octaphyrins exhibit different conformations, such as figure-eight, twisted, or planar, depending on the nature of the linkages, the number of *meso* carbon bridges, and the steric bulk of the *meso* aryl substituents. To the best of our knowledge, all of the octaphyrins with six *meso* carbons reported in the literature[16] adopt figure-eight conformations, and this is the first report in which a modified octaphyrin with six *meso* links has a planar conformation. The rigid terthiophene subunit plays an important role here in achieving the planar conformation. Recently we have reported a planar aromatic octaphyrin containing a rigid quaterthiophene subunit with two heterocyclic rings inverted both in the free base and the protonated forms.[17] Figure 7 (a) shows that one of the terminal thiophene rings (A) of the terthiophene subunit

and another thiophene ring (E) of the tripyrrane subunit are inverted. One pyrrole ring (F) is also inverted, with NH pointing outside of the macrocycle. The molecules deviate slightly from planarity, as can be seen in side view (Figure 7, b). The dihedral angles of the heterocyclic rings (A, B, C, D, E, F, G, H) with respect to the mean plane defined by the six *meso* carbon atoms are 21.52°, 13.04°, 9.06°, 8.29°, 7.61°, 5.20°, 6.56°, and 13.79°, respectively. The bond alternation of the conjugated double bond is evident from the X-ray structure, in line with the assignment as a 36π electron nonaromatic system. The single-crystal X-ray structure of TFA-bound rubyrin **19** has been given in a preliminary communication[10b] (CCDC-612135, see supporting information). In the rubyrin, the thiophene ring opposite to the terthiophene unit is inverted. There are two molecules in an asymmetric unit and two C–H···O interactions [C6–H6···O8, 2.37 Å, 152°; C10–H10···O6, 2.42 Å, 169°] in one of the molecule. There is one more C–H···O interaction [C70–H70···O1, 2.49 Å, 163°] with the other molecule present in the asymmetric unit (see supporting information).

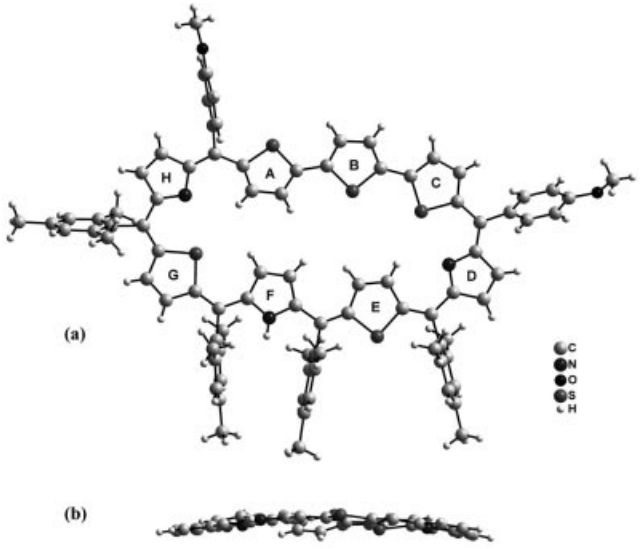

Figure 7. Single-crystal X-ray structure of **30**: top view (a) and its side view (b). The *meso* substituents in the side view are removed for clarity.

All attempts to obtain crystal structures of the dodecaphyrins failed. Therefore, the structural features of this system were determined with the help of theoretical analysis at both semiempirical and density functional theory (DFT) levels. The various conformational possibilities tested for unsubstituted dodecaphyrin are presented in Figure 8, along with their relative heats of formation. A planar configuration of the system similar to that shown in Scheme 2 is highly unlikely, as it would suffer from ring strain due to the large angle of 144 ° observed for the sp^2-hybridized *meso* carbon atom (Figure 8, a). This implies that the system would adopt nonplanar structures through the adoption of appropriate distortions at the *meso* junctions. This is indeed true, as all the nonplanar structures showed much higher stabilities than the planar structure given in Figure 8 (a). Interestingly, among the nonplanar structures, the 'figure-eight' structure (Figure 8, d) is the most stable. On the basis of this finding, the full model of this system was constructed and optimized at the B3LYP/6-31G* level of DFT using the Gaussian suite of programs.[18,19] The DFT level structure is presented in Figure 9 along with some selected bond lengths.

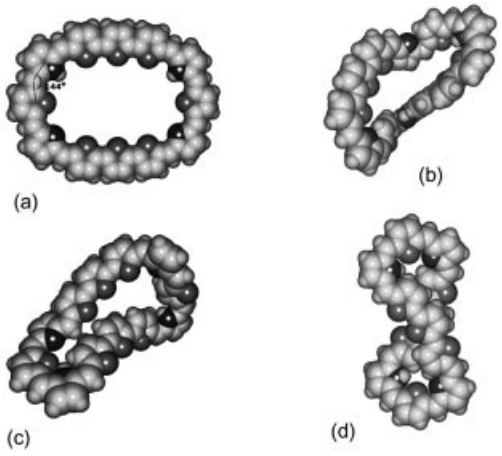

Figure 8. Different conformations of the dodecaphyrin **28**. The relative heats of formations are **a**) 145.2, **b**) 10.7, **c**) 8.0, and **d**) 0.0 kcal mol^{-1}.

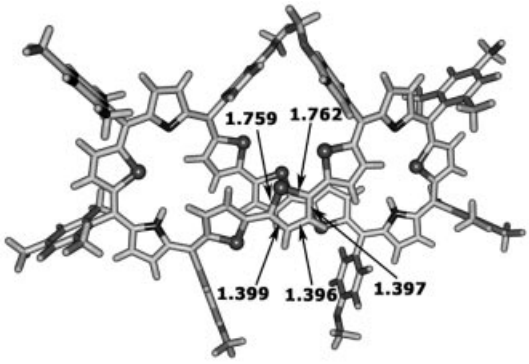

Figure 9. Optimized structure of fully substituted dodecaphyrin **28**, at B3LYP/6-31G* level showing the 'figure-eight' configuration. The bond lengths shown are in Å.

Electrochemical Studies

The redox behavior of various conjugates was monitored by cyclic voltammetric studies using $TBAPF_6$ (tetra *n*-butylammonium hexafluorophosphate, 0.1 M) as the supporting electrolyte in CH_2Cl_2 in the 0 to 1.6 V potential range vs. standard calomel electrode at 100 mV s^{-1} scan speed. In general, rubyrins, octaphyrins, and dodecaphyrins each show two quasireversible oxidations. The electrochemical data for these expanded porphyrins are listed in Table 1. Comparison of the redox data reveal several interesting observations: a) a significant decrease in the first oxidation potential as the number of conjugated π electrons increases in the macrocycle, suggesting destabilization in the HOMO, b) replacement of S with Se in the core of the macrocycle leads to an increase in the oxidation potential, and c) sub-

stitution of an electron-donating *meso* aryl group leads to easy oxidation of macrocycle. Some typical cyclic voltammograms overlayed with differential pulse voltammograms of these expanded porphyrins are shown in the electronic supporting information.

Table 1. Electrochemical data for rubyrins, hexaphyrins, and dodecaphyrins with $TBAF_6$ (0.1 M) as the supporting electrolyte in CH_2Cl_2, potential scanned from 0–1.6 V vs. SCE recorded at 100 mV s^{-1} scan speed.

Compound	$E_{1/2}^{ox}$ (1) /V	$E_{1/2}^{ox}$ (2) /V
15	0.700	1.20
16	0.702	1.203
17	0.692	1.121
18	0.694	1.124
19	0.674	1.068
20	0.680	1.106
21	0.665	1.045
22	0.671	1.02
23	0.660	1.032
24	0.656	0.960
26	0.684	1.10
27	0.687	1.116
28	0.280	0.696
29	0.288	0.706
30	0.300	0.504
31	0.309	0.510

Two-Photon Absorption Properties

The third-order nonlinear optical properties of the porphyrins described above were followed through measurement of two-photon absorption cross-section (TPACS) $\sigma^{(2)}$ values using the open aperture Z-scan method.[14] The TPA spectra were measured at 780 nm using 100 fs pulses for rubyrins **15**–**27**, and at 870 nm using 100 fs pulses for octaphyrins **30** and **31** and dodecaphyrins **28** and **29**. All of the samples were measured in 10^{-4} M solutions in CH_2Cl_2 and showed negligible single-photon absorptions at the respective wavelengths. The solvent itself does not show any TPA under the experimental conditions. The general features of these finding are as follows. The TPACS values measured by the open aperture Z-scan method depend on:

i) The effect of π conjugation; $\sigma^{(2)}$ increases as we go from 26π to the 54π systems. A $\sigma^{(2)}$ value of 12280 GM was observed for rubyrin **23**, 42980 GM for octaphyrin **30**, and 89560 GM for dodecaphyrin **28**.

ii) The effect of core heteroatoms (S vs. Se); replacement of S with Se in the core of the macrocycle reduces the symmetry of the macrocycle and this may be responsible for decreasing the $\sigma^{(2)}$ values. For example, rubyrin **15** showed a larger $\sigma^{(2)}$ value of 4240 GM than **16** (2800 GM), octaphyrin **30** showed a larger $\sigma^{(2)}$ value of 42980 GM than **31** (23420 GM), and dodecaphyrin **28** showed a larger $\sigma^{(2)}$ value of 89560 GM than **29** (69710 GM).

iii) The effect of the presence of *meso*-aryl substituents on the macrocycle; $\sigma^{(2)}$ values increase with increasingly electron-donating natures of the substituents in the same type of conjugated macrocycles.

The details of these observations are summarized in Table 2.

Table 2. TPA cross-section values of rubyrins, octaphyrins, and dodecaphyrins measured by femtosecond laser pulses.

Compound	TPA cross-section ($\sigma^{(2)}$) values (GM)
15	4240
16	2800
17	5760
18	4840
19	5970
20	5580
21	10780
22	8370
23	12280
24	15250
26	5820
27	5140
28	89560
29	69710
30	42980
31	23420

Conclusion

In summary, we have described the syntheses of three new, heteroatom-substituted, core-modified [26]rubyrin, [36]octaphyrin, and [54]dodecaphyrin systems. The natures of the expanded porphyrins and their structures depend on the *meso* substituents present on the precursors and the acid concentrations used in the reactions. We have shown that through changing the *meso* aryl substituents and controlling the concentration of acid catalyst it is possible to generate new expanded porphyrins containing 26π, 36π, and 54π electron systems in one-pot reactions. The rigid terthiophene subunit helps in avoiding figure-eight conformations and in achieving planar conformations in octaphyrins. These core-modified expanded porphyrins can be regarded as one of the best suitable candidates, especially as organic nonlinear optical materials, due to their exceptionally large two-photon absorption cross-sections. Further studies to apply this strategy in syntheses of other novel expanded porphyrins and their anion and cation binding to exploit their application as receptors are currently in progress.

Experimental Section

Instrumentation: Electronic spectra were recorded on a Perkin–Elmer Lambda 20 UV/Vis spectrophotometer. Proton NMR spectra for hexaphyrins and octaphyrins were obtained on a JEOL 300 MHz in $CDCl_3$ and those for dodecaphyrins were recorded on a Bruker Avance DRX 500 MHz spectrometer in CD_2Cl_2. FAB-MS spectra were obtained on a JEOL-SX-120/DA6000 spectrometer. All CV experiments were performed with a PAR 273 potentiostat (EG&G, US) at room temperature. Inert conditions were achieved by bubbling Ar before each measurement. A standard three-electrode arrangement of a platinum (Pt) wire as the working electrode, a platinum coil as the counter electrode, and a calomel reference electrode was used. TPA cross-section values [$\sigma^{(2)}$] were measured by using a standard open aperture Z-scan method[14] for 1 cm long sample cells with 50 MHz repetition rates from a Femtolite laser (IMRA) operating at the second-harmonic wavelength of the Er-doped fiber laser. The 20 cm lens used for the Z-scan experi-

ments produce GW-level laser intensities at the focus, which easily induces two-photon absorption.

Chemicals: All NMR solvents were used as received. Most of the syntheses were carried out under nitrogen. The CH_2Cl_2 used for synthesis and cyclic voltammetry was dried (P_2O_5), distilled from CaH_2, and stored over molecular sieves (4 Å). Solvents such as tetrahydrofuran and *n*-hexane were dried with sodium/benzoquinone. Tetra-*n*-butylammonium hexafluorophosphate from Fluka was used as the supporting electrolyte for cyclic voltammetry studies. Terthiophene diols and tripyrranes were synthesized by published procedure and stored under inert atmospheres.[9,15]

General Procedure for the Syntheses of Rubyrins

Compound 15: A mixture of **7** (0.3 g, 0.55 mmol) and tripyrrane **11** (0.265 g, 0.55 mmol) was dissolved in dry dichloromethane (200 mL) and stirred under nitrogen for 5 min. *p*-Toluenesulfonic acid (PTSA) (0.030 g, 0.165 mmol) was added and the stirring was continued for 90 min. Chloranil (0.410 g, 1.65 mmol) was added and the reaction mixture was exposed to air and heated at reflux for a further 90 min. The solvent was evaporated in vacuo. The residue was purified by chromatography on a basic alumina column; the first red band that eluted with dichloromethane/petroleum ether (1:4) gave **15** (0.110 g, 22.2%). ^{1}H NMR (300 MHz, $CDCl_3$, 25 °C, TMS): δ = 9.79 (s, 2 H), 9.64 (d, J = 4.3 Hz, 2 H), 9.20 (d, J = 4.3 Hz, 2 H), 8.18 (d, J = 4.5 Hz, 2 H), 8.17 (d, J = 7.8 Hz, 4 H), 7.78 (m, 6 H), 7.70 (d, J = 4.5 Hz, 2 H), 7.22 (s, 4 H), 2.56 (s, 6 H), 2.02 (s, 12 H) ppm. UV/Vis (CH_2Cl_2): λ_{max} (ε) = 529 (19.0), 668 (2.4), 722 nm (4.2×10^{-4} M^{-1} cm^{-1}); (CH_2Cl_2/TFA): λ_{max} (ε) = 560 (21.7), 608 (12.6), 822 (4.3), 907 nm (5.8×10^{-4} M^{-1} cm^{-1}). FAB-MS: *m*/*z* (%) = 897 (100) [M + H]$^+$. $C_{58}H_{44}N_2S_4$ (897.24): calcd. C 77.64, H 4.94, N 3.12; found C 77.41, H 4.89, N 3.31.

Compound 16: Yield 0.126 g, 23.1%. ^{1}H NMR (300 MHz, $CDCl_3$, 25 °C, TMS): δ = 9.61 (s, 2 H), 9.45 (d, J = 4.3 Hz, 2 H), 9.02 (d, J = 4.3 Hz, 2 H), 8.11 (m, 4 H), 8.05 (d, J = 4.5 Hz, 2 H), 7.75 (m, 6 H), 7.52 (d, J = 4.5 Hz, 2 H), 7.20 (s, 4 H), 2.54 (s, 6 H), 2.12 (s, 12 H) ppm. UV/Vis (CH_2Cl_2): λ_{max} (ε) = 533 (13.5), 607 (1.4), 663 (1.7), 718 nm (2.5×10^{-4} M^{-1} cm^{-1}); (CH_2Cl_2/TFA): λ_{max} (ε) = 564 (17.7), 607 (8.7), 827 (3.0), 909 nm (3.4×10^{-4} M^{-1} cm^{-1}). FAB-MS: *m*/*z* (%) = 945 (100) [M + H]$^+$. $C_{58}H_{44}N_2S_3Se$ (944.14): calcd. C 73.78, H 4.70, N 2.97; found C 73.61, H 4.80, N 2.91.

Compound 17: (0.1 g, yield 21.4%). ^{1}H NMR (300 MHz, $CDCl_3$, 25 °C, TMS): δ = 9.77 (s, 2 H), 9.61 (d, J = 4.3 Hz, 2 H), 9.20 (d, J = 4.3 Hz, 2 H), 8.19 (d, J = 4.5 Hz, 2 H), 8.07 (d, J = 7.8 Hz, 4 H), 7.67 (d, J = 4.5 Hz, 2 H), 7.59 (d, J = 7.8 Hz, 4 H), 7.21 (s, 4 H), 2.68 (s, 6 H), 2.56 (s, 6 H), 2.08 (s, 12 H) ppm. UV/Vis (CH_2Cl_2): λ_{max} (ε) = 530 (23.6), 669 (2.9), 722 nm (5.3×10^{-4} M^{-1} cm^{-1}); (CH_2Cl_2/TFA): λ_{max} (ε) = 562 (26.4), 608 (14.3), 824 (5.1), 908 nm (7.2×10^{-4} M^{-1} cm^{-1}). FAB-MS: *m*/*z* (%) = 925 (100) [M + H]$^+$. $C_{60}H_{48}N_2S_4$ (925.29): calcd. C 77.88, H 5.23, N 3.03; found C 77.71, H 5.29, N 3.11.

Compound 18: Yield 0.131 g, 24.6%. ^{1}H NMR (300 MHz, $CDCl_3$, 25 °C, TMS): δ = 9.57 (s, 2 H), 9.41 (d, J = 4.3 Hz, 2 H), 9.02 (d, J = 4.3 Hz, 2 H), 8.05 (d, J = 4.5 Hz, 2 H), 8.01 (d, J = 7.8 Hz, 4 H), 7.56 (d, J = 7.8 Hz, 4 H), 7.48 (d, J = 4.5 Hz, 2 H), 7.19 (s, 4 H), 2.66 (s, 6 H), 2.54 (s, 6 H), 2.12 (s, 12 H) ppm. UV/Vis (CH_2Cl_2): λ_{max} (ε) = 534 (13.0), 608 (1.3), 664 (1.6), 720 nm (2.4×10^{-4} M^{-1} cm^{-1}); (CH_2Cl_2/TFA): λ_{max} (ε) = 566 (15.9), 608 (8.3), 827 (2.9), 911 nm (3.7×10^{-4} M^{-1} cm^{-1}). FAB-MS: *m*/*z* (%) = 973 (100) [M + H]$^+$. $C_{60}H_{48}N_2S_3Se$ (972.19): calcd. C 74.13, H 4.98, N 2.88; found C 74.41, H 4.89, N 2.91.

Compound 19: Yield 0.119 g, 23.9%. ^{1}H NMR (300 MHz, $CDCl_3$, 25 °C, TMS): δ = 9.70 (s, 2 H), 9.61 (d, J = 4.2 Hz, 2 H), 8.97 (d, J = 4.2 Hz, 2 H), 8.01 (d, J = 4.5 Hz, 2 H), 7.62 (d, J = 4.5 Hz, 2 H), 7.26 (s, 4 H), 7.21 (s, 4 H), 2.60 (s, 6 H), 2.55 (s, 6 H), 2.09 (s, 12 H), 2.08 (s, 12 H) ppm. UV/Vis (CH_2Cl_2): λ_{max} (ε) = 527 (19.7), 662 (2.5), 717 nm (4.2×10^{-4} M^{-1} cm^{-1}); (CH_2Cl_2/TFA): λ_{max} (ε) = 557 (26.2), 606 (16.1), 821 (4.8), 906 nm (5.8×10^{-4} M^{-1} cm^{-1}). FAB-MS: *m*/*z* (%) = 981 (100) [M + H]$^+$. $C_{64}H_{56}N_2S_4$ (981.40): calcd. C 78.32, H 5.75, N 2.85; found C 78.41, H 5.59, N 2.71.

Compound 20: Yield 0.102 g, 21.2%. ^{1}H NMR (300 MHz, $CDCl_3$, 25 °C, TMS): δ = 9.55 (s, 2 H), 9.39 (d, J = 4.2 Hz, 2 H), 8.80 (d, J = 4.2 Hz, 2 H), 7.88 (d, J = 4.5 Hz, 2 H), 7.44 (d, J = 4.5 Hz, 2 H), 7.24 (s 4 H), 7.18 (s, 4 H), 2.58 (s, 6 H), 2.54 (s, 6 H), 2.13 (s, 12 H), 2.08 (s, 12 H) ppm. UV/Vis (CH_2Cl_2): λ_{max} (ε) = 532 (11.6), 607 (1.2), 659 (1.5), 713 nm (2.0×10^{-4} M^{-1} cm^{-1}); (CH_2Cl_2/TFA): λ_{max} (ε) = 562 (17.0), 607 (9.8), 825 (3.0), 909 nm (3.2×10^{-4} M^{-1} cm^{-1}). FAB-MS: *m*/*z* (%) = 1029 (100) [M + H]$^+$. $C_{64}H_{56}N_2S_3Se$ (1028.30): calcd. C 74.75, H 5.49, N 2.72; found C 74.41, H 5.59, N 2.61.

Compound 21: Yield 0.105 g, 23.3%. ^{1}H NMR (300 MHz, $CDCl_3$, 25 °C, TMS): δ = 9.78 (s, 2 H), 9.62 (d, J = 4.3 Hz, 2 H), 9.24 (d, J = 4.3 Hz, 2 H), 8.21 (d, J = 4.5 Hz, 2 H), 8.11 (d, J = 8.2 Hz, 4 H), 7.80 (d, J = 8.2 Hz, 4 H), 7.67 (d, J = 4.5 Hz, 2 H), 7.22 (s, 4 H), 2.57 (s, 6 H), 2.08 (s, 12 H), 1.59 (s, 18 H) ppm. UV/Vis (CH_2Cl_2): λ_{max} (ε) = 530 (16.6), 669 (2.1), 725 nm (3.8×10^{-4} M^{-1} cm^{-1}); (CH_2Cl_2/TFA): λ_{max} (ε) = 563 (18.9), 608 (9.9), 825 (3.6), 910 (5.1×10^{-4} M^{-1} cm^{-1}). FAB-MS: *m*/*z* (%) = 1009 (100) [M + H]$^+$. $C_{66}H_{60}N_2S_4$ (1009.45): calcd. C 78.53, H 5.99, N 2.78; found C 78.41, H 5.89, N 2.61.

Compound 22: Yield 0.132 g, 22.3%. ^{1}H NMR (300 MHz, $CDCl_3$, 25 °C, TMS): δ = 9.58 (s, 2 H), 9.42 (d, J = 4.3 Hz, 2 H), 9.06 (d, J = 4.3 Hz, 2 H), 8.08 (d, J = 4.5 Hz, 2 H), 8.06 (d, J = 8.2 Hz, 4 H), 7.77 (d, J = 8.2 Hz, 4 H), 7.49 (d, J = 4.5 Hz, 2 H), 7.19 (s, 4 H), 2.55 (s, 6 H), 2.12 (s, 12 H), 1.57 (s, 18 H) ppm. UV/Vis (CH_2Cl_2): λ_{max} (ε) = 534 (15.5), 608 (1.7), 665 (1.9), 721 nm (2.9×10^{-4} M^{-1} cm^{-1}); (CH_2Cl_2/TFA): λ_{max} (ε) = 571 (25.8), 767 (1.7), 840 (3.8), 911 nm (1.8×10^{-4} M^{-1} cm^{-1}). FAB-MS: *m*/*z* (%) = 1057 (100) [M + H]$^+$. $C_{66}H_{60}N_2S_3Se$ (1056.35): calcd. C 75.04, H 5.73, N 2.65; found C 75.21, H 5.89, N 2.51.

Compound 23: Yield 0.1 g, 20.8%. ^{1}H NMR (300 MHz, $CDCl_3$, 25 °C, TMS): δ = 9.92 (s, 2 H), 9.78 (d, J = 4.3 Hz, 2 H), 9.14 (d, J = 4.3 Hz, 2 H), 8.14 (d, J = 4.5 Hz, 2 H), 8.05 (d, J = 7.7 Hz, 4 H), 7.91 (d, J = 4.5 Hz, 2 H), 7.53 (d, J = 7.7 Hz, 4 H), 7.29 (s, 4 H), 2.65 (s, 6 H), 2.62 (s, 6 H), 2.06 (s, 12 H) ppm. UV/Vis (CH_2Cl_2): λ_{max} (ε) = 533 (12.0), 608 (1.3), 667 (1.4), 722 nm (2.1×10^{-4} M^{-1} cm^{-1}); (CH_2Cl_2/TFA): λ_{max} (ε) = 564 (15.7), 609 (8.6), 834 (2.7), 912 nm (2.8×10^{-4} M^{-1} cm^{-1}). FAB-MS: *m*/*z* (%) = 925 (100) [M + H]$^+$. $C_{60}H_{48}N_2S_4$ (925.29): calcd. C 77.88, H 5.23, N 3.03; found C 77.41, H 5.28, N 3.11.

Compound 24: Yield 0.109 g, 20.9%. ^{1}H NMR (300 MHz, $CDCl_3$, 25 °C, TMS): δ = 9.71 (s, 2 H), 9.56 (d, J = 4.3 Hz, 2 H), 8.95 (d, J = 4.3 Hz, 2 H), 8.00 (d, J = 4.5 Hz, 2 H), 7.98 (d, J = 7.8 Hz, 4 H), 7.69 (d, J = 4.5 Hz, 2 H), 7.49 (d, J = 7.8 Hz, 4 H), 7.26 (s, 4 H), 2.64 (s, 6 H), 2.60 (s, 6 H), 2.06 (s, 12 H) ppm. UV/Vis (CH_2Cl_2): λ_{max} (ε) = 529 (11.1), 608 (0.9), 672 (1.3), 727 nm (2.4×10^{-4} M^{-1} cm^{-1}); (CH_2Cl_2/TFA): λ_{max} (ε) = 559 (13.3), 610 (7.1), 834 (2.4), 909 nm (2.7×10^{-4} M^{-1} cm^{-1}). FAB-MS: *m*/*z* (%) = 973 (100) [M + H]$^+$. $C_{60}H_{48}N_2S_3Se$ (972.19): calcd. C 74.13, H 4.98, N 2.88; found C 74.31, H 4.89, N 2.95.

Compound 26: Yield 0.06 g, 2.8%. ^{1}H NMR (300 MHz, $CDCl_3$, 25 °C, TMS): δ = 9.35 (s, 2 H), 9.21 (d, J = 4.3 Hz, 2 H), 8.89 (d, J = 4.3 Hz, 2 H), 7.95 (d, J = 4.5 Hz, 2 H), 7.90 (d, J = 8.6 Hz, 4 H), 7.25 (d, J = 4.5 Hz, 2 H), 7.21 (d, J = 8.6 Hz, 4 H), 7.12 (s, 4

H), 4.02 (s, 6 H), 2.50 (s, 6 H), 2.08 (s, 12 H) ppm. UV/Vis (CH_2Cl_2): λ_{max} (ε) = 531 (19.8), 672 (2.7), 726 nm (3.5×10^{-4} M^{-1} cm^{-1}); (CH_2Cl_2/TFA): λ_{max} (ε) = 564 (21.2), 609 (13.0), 825 (4.8), 911 nm (6.8×10^{-4} M^{-1} cm^{-1}). FAB-MS: *m/z* (%) = 957 (100) $[M + H]^+$. $C_{60}H_{48}N_2O_2S_4$ (957.29): calcd. C 75.28, H 5.05, N 2.93; found C 75.32, H 5.19, N 2.81.

Compound 27: Yield 0.065 g, 14.9%. ^{1}H NMR (300 MHz, $CDCl_3$, 25 °C, TMS): δ = 9.55 (s, 2 H), 9.39 (d, J = 4.3 Hz, 2 H), 9.01 (d, J = 4.3 Hz, 2 H), 8.06 (d, J = 4.5 Hz, 2 H), 8.05 (d, J = 8.6 Hz, 4 H), 7.47 (d, J = 4.5 Hz, 2 H), 7.29 (d, J = 8.6 Hz, 4 H), 7.19 (s, 4 H), 4.07 (s, 6 H), 2.54 (s, 6 H), 2.12 (s, 12 H) ppm. UV/Vis (CH_2Cl_2): λ_{max} (ε) = 535 (15.9), 610 (1.8), 667 (2.0), 722 nm (3.2×10^{-4} M^{-1} cm^{-1}); (CH_2Cl_2/TFA): λ_{max} (ε) = 573 (19.2), 606 (8.9), 834 (3.7), 913 nm (3.8×10^{-4} M^{-1} cm^{-1}). FAB-MS: *m/z* (%) = 1005 (100) $[M + H]^+$. $C_{60}H_{48}N_2O_2S_3Se$ (1004.19): calcd. C 71.76, H 4.82, N 2.79; found C 71.41, H 4.89, N 2.31.

General Procedure for the Synthesis of Dodecaphyrins

Compound 28: Compound **25** (0.300 g, 0.057 mmol) and tripyrrane **11** (0.310 g, 0.057 mmol) were subjected to conditions similar to those described above with PTSA (0.030 g, 0.017 mmol) and chloranil (0.041 g, 1.65 mmol). Purification by column chromatography on basic alumina gave a red-colored band identified as rubyrin **26** with dichloromethane/petroleum ether (1:4), together with a blue band moving with dichloromethane/petroleum ether (2:3), which on evaporation of solvent yielded a brownish metallic solid, identified as **28** (0.02 g, 6%). FAB-MS: *m/z* (%) = 1916 (100) $[M]^+$. UV/Vis (CH_2Cl_2): λ_{max} (ε) = 604 (11.6), 744 nm (3.2×10^{-4} M^{-1} cm^{-1}); (CH_2Cl_2/TFA): λ_{max} (ε) = 710 (18.2), 842 (2.2), 965 nm (4.7×10^{-4} M^{-1} cm^{-1}). $C_{120}H_{98}N_4O_4S_8$ (1916.56): calcd. C 75.20, H 5.15, N 2.92; found C 75.11, H 5.99, N 2.81

Compound 29: Yield 0.029 g, 7.8%. UV/Vis (CH_2Cl_2): λ_{max} (ε) = 606 (10.9), 746 nm (3.5×10^{-4} M^{-1} cm^{-1}); (CH_2Cl_2/TFA): λ_{max} (ε) = 726 (19.2), 845 (2.4), 970 nm (4.9×10^{-4} M^{-1} cm^{-1}). FAB-MS: *m/z* (%) = 2012 (100) $[M + 2H]^+$. $C_{120}H_{98}N_4O_4S_6Se_2$ (2010.39): calcd. C 71.69, H 4.91, N 2.79; found C 71.61, H 4.89, N 2.71

General Procedure for the Synthesis of Octaphyrins

Compound 30: Compound **25** (0.300 g, 0.057 mmol) and tripyrrane **11** (0.310 g, 0.057 mmol) were subjected to conditions similar to those described above with PTSA (0.060 g, 0.034 mmol) and chloranil (0.041 g, 1.65 mmol). Purification by column chromatography on basic alumina gave a violet-colored band with dichloromethane/petroleum ether (1:10) identified as octaphyrin **30** (0.04 g, 10%). The second band, moving with dichloromethane/petroleum ether (1:4), was identified as rubyrin **26** (0.05 g, 10%), and a blue band, moving with dichloromethane/petroleum ether (2:3), yielded a brownish metallic solid identified on evaporation of solvent as **28** (0.02 g, 6%).

Compound 30: ^{1}H NMR (300 MHz, $CDCl_3$, 25 °C, TMS): δ = 12.73 (d, J = 6.0 Hz, 1 H), 12.52 (d, J = 4.0 Hz, 1 H), 11.10 (d, J = 6.0 Hz, 1 H), 10.68 (d, J = 4.0 Hz, 1 H), 10.50 (d, J = 3.8 Hz, 1 H), 10.07 (d, J = 3.8 Hz, 1 H), 7.17 (d, J = 8.6 Hz, 2 H), 7.10 (d, J = 8.6 Hz, 2 H), 6.82 (d, J = 8.7 Hz, 2 H), 6.80 (d, J = 8.7 Hz, 2 H), 6.78 (s, 2 H), 6.68 (s, 2 H), 6.52 (s, 2 H), 6.47 (s, 2 H), 6.29 (t, 2 H), 6.22 (d, J = 3.9 Hz, 1 H), 6.12 (d, J = 3.9 Hz, 1 H), 5.98 (t, 2 H), 5.46 (d, J = 4.7 Hz, 1 H), 5.43 (d, J = 5.5 Hz, 1 H), 5.36 (d, J = 5.5 Hz, 1 H), 5.29 (d, J = 4.7 Hz, 1 H), 5.26 (br. s, 1 H), 3.80 (d, 6 H), 2.21 (s, 3 H), 2.13 (d, 6 H), 2.08 (s, 15 H), 1.87 (s, 12 H) ppm. UV/Vis (CH_2Cl_2): λ_{max} (ε) = 525 (11.3), 613 nm (5.2×10^{-4} M^{-1} cm^{-1}); (CH_2Cl_2/TFA): λ_{max} (ε) = 622 (15.2), 702 (10.1). FAB-MS: *m/z* (%) = 1366 (100) $[M]^+$. $C_{88}H_{75}N_3O_2S_5$ (1366.88): calcd. C 77.32, H 5.53, N 3.07; found C 77.26, H 5.59, N 3.01.

Compound 31: Yield 0.047 g, 11.5%. ^{1}H NMR (300 MHz, $CDCl_3$, 25 °C, TMS): δ = 12.17 (d, J = 6.0 Hz, 1 H), 11.88 (d, J = 4.0 Hz, 1 H), 10.62 (d, J = 6.0 Hz, 1 H), 10.08 (d, J = 4.0 Hz, 1 H), 9.77 (d, J = 3.8 Hz, 1 H), 9.57 (d, J = 3.8 Hz, 1 H), 7.72 (d, J = 8.6 Hz, 2 H), 7.69 (d, J = 8.6 Hz, 2 H), 7.55 (d, J = 8.7 Hz, 2 H), 7.53 (d, J = 8.7 Hz, 2 H), 7.36 (s, 2 H), 7.31 (s, 2 H), 7.23 (s, 2 H), 7.20 (s, 2 H), 7.14 (m, 4 H), 6.85 (d, 2 H), 6.82 (d, 2 H), 5.36 (d, J = 5.5 Hz, 1 H), 5.29 (d, J = 4.7 Hz, 1 H), 5.26 (br. s, 1 H), 3.80 (d, 6 H), 2.21 (s, 3 H), 2.13 (d, 6 H), 2.08 (s, 15 H), 1.87 (s, 12 H) ppm. UV/Vis (CH_2Cl_2): λ_{max} (ε) = 525 (11.3), 613 (5.2×10^{-4} M^{-1} cm^{-1}); (CH_2Cl_2/TFA): λ_{max} (ε) = 622 (14.9), 701 nm (9.8×10^{-4} M^{-1} cm^{-1}). FAB-MS: *m/z* (%) = 1461 (100) $[M]^+$. $C_{88}H_{75}N_3O_2S_3Se_2$ (1460.88): calcd. C 77.36, H 5.18, N 2.88; found C 77.30, H 5.19, N 3.03.

Supporting Information (see also the footnote on the first page of this article): Ortep diagram of rubyrin **19**, ^{1}H NMR and ^{1}H-^{1}H COSY spectra of rubyrins **19** and **24** and octaphyrin **30**, FAB mass spectra of **28**–**31** and cyclic voltammograms of **18**, **30**, and **28.**

Acknowledgments

T. K. C. thanks the Department of Science and Technology (DST) for a J. C. Bose fellowship and the Council of Scientific and Industrial Research (CSIR), Government of India, New Delhi for a research grant. R. K. thanks the CSIR for a Shyama Prasad Mukherjee fellowship. R. M. and A. N. thank the CSIR and the UGC, respectively, for their fellowships. D. G. thanks DST, MCIT, New Delhi, and the International SRF programme of the Welcome Trust, UK for financial support.

[1] a) M. Shionoya, H. Furuta, V. Lynch, A. Harriman, J. L. Sessler, *J. Am. Chem. Soc.* **1992**, *114*, 5714–5722; b) J. L. Sessler, J. M. Davis, *Acc. Chem. Res.* **2001**, *34*, 989–997; c) J. L. Sessler, A. Gebauer, S. J. Weghorn, *The Porphyrin Handbook* (Ed.: K. M. Kadish), *Expanded Porphyrins*, Academic Press: San Diego, **2000**, vol. 2, pp. 1–54 and references cited therein; d) T. K. Chandrashekar, S. Venkatraman, *Acc. Chem. Res.* **2003**, *36*, 676–691; e) J. L. Sessler, A. Gebauer, S. J. Weghorn, *Expanded Porphyrins* (Eds.: K. M. Kadish, K. M. Smith, R. Guilard), San Diego, **2000**, vol. 2, pp. 55–121; f) A. Jasat, D. Dolphin, *Chem. Rev.* **1997**, *97*, 2267–2340.

[2] a) R. Charrière, T. A. Jenny, H. Rexhausen, A. Gossauer, *Heterocycles* **1993**, *36*, 1561–1575; b) A. Werner, M. Michels, L. Zander, J. Lex, E. Vogel, *Angew. Chem.* **1999**, *111*, 3866–3870; *Angew. Chem. Int. Ed.* **1999**, *38*, 3650–3653; c) S. J. Weghorn, J. L. Sessler, V. Lynch, T. F. Baumann, J. W. Sibert, *Inorg. Chem.* **1996**, *35*, 1089–1090.

[3] a) A. Harriman, B. G. Maiya, T. Murai, G. Hemmi, J. L. Sessler, T. E. Mallouk, *J. Chem. Soc. Chem. Commun.* **1989**, 314–316; b) B. G. Maiya, A. Harriman, J. L. Sessler, G. Hemmi, T. Murai, T. E. Mallouk, *J. Phys. Chem.* **1989**, *93*, 8111–8115.

[4] J. L. Sessler, T. D. Mody, G. W. Hemmi, V. Lynch, S. W. Young, R. A. Miller, *J. Am. Chem. Soc.* **1993**, *115*, 10368–10369.

[5] a) T. K. Ahn, J. H. Kwon, D. Y. Kim, D. W. Cho, D. H. Jeong, S. K. Kim, M. Suzuki, S. Shimizu, A. Osuka, D. Kim, *J. Am. Chem. Soc.* **2005**, *127*, 12856–12861; b) H. Rath, J. Sankar, V. PrabhuRaja, T. K. Chandrashekar, A. Nag, D. Goswami, *J. Am. Chem. Soc.* **2005**, *127*, 11608–11609; c) R. Misra, R. Kumar, T. K. Chandrashekar, C. H. Suresh, A. Nag, D. Goswami, *J. Am. Chem. Soc.* **2006**, *128*, 16083–16091; d) M. R. Marder, B. Kippelen, A. K.-Y. Jen, N. Peyghambarian, *Nature* **1997**, *388*, 845–851; e) W. Zhou, S. M. Kuebler, K. L. Braun, T. Yu, J. K. Cammack, C. K. Ober, J. W. Perry, S. R. Marder, *Science* **2002**, *296*, 1106–1109.

[6] S. J. Narayanan, A. Srinivasan, B. Sridevi, T. K. Chandrashekar, M. O. Senge, K.-I. Sugiura, Y. Sakata, *Eur. J. Org. Chem.* **2000**, 2357–2360.
[7] a) A. Srinivasan, V. M. Reddy, S. J. Narayanan, B. Sridevi, S. K. Pushpan, M. R. Kumar, T. K. Chandrashekar, *Angew. Chem. Int. Ed. Engl.* **1997**, *36*, 2598–2601; b) A. Srinivasan, S. K. Pushpan, M. R. Kumar, T. K. Chandrashekar, R. Roy, *Tetrahedron* **1999**, *55*, 6671–6680; c) S. K. Pushpan, V. G. Anand, S. Venkatraman, A. Srinivasan, A. K. Gupta, T. K. Chandrashekar, *Tetrahedron Lett.* **2001**, *42*, 3391–3394.
[8] J. L. Sessler, D. Seidel, C. Bucher, V. Lynch, *Chem. Commun.* **2000**, 1473–1474.
[9] V. G. Anand, S. K. Pushpan, A. Srinivasan, S. J. Narayanan, B. Sridevi, T. K. Chandrashekar, R. Roy, B. S. Joshi, *Org. Lett.* **2000**, *2*, 3829–3832.
[10] a) A single-crystal X-ray structure was also obtained for free base **19**. Even though the *R* factor was high (0.1921) for the structure and detailed bond length and bond angle analysis could not be done, the core structure was found to be the same as in the TFA-bound form; b) R. Kumar, R. Misra, T. K. Chandrashekar, *Org. Lett.* **2006**, *8*, 4847–4850.
[11] a) T. D. Lash, S. T. Chaney, D. T. Ritcher, *J. Org. Chem.* **1998**, *63*, 9076–9088; b) J. S. Lindsey, R. W. Wagner, *J. Org. Chem.* **1989**, *54*, 828–836; c) C. H. Lee, J. S. Lindsey, *Tetrahedron* **1994**, *50*, 11427–11440; d) V. G. Anand, S. K. Pushpan, S. Venkatraman, S. J. Narayanan, A. Dey, T. K. Chandrashekar, R. Roy, B. S. Joshi, S. Deepa, G. N. Sastry, *J. Org. Chem.* **2002**, *67*, 6309–6319; e) S. J. Narayanan, Ph.D. Thesis, Indian Institute of Technology, Kanpur, **2000**.
[12] S. J. Narayan, B. Sridevi, T. K. Chandrashekar, A. Vij, R. Roy, *J. Am. Chem. Soc.* **1999**, *121*, 9053–9068.
[13] V. G. Anand, S. Venkatraman, H. Rath, T. K. Chandrashekar, W. Teng, K. R. Senge, *Chem. Eur. J.* **2003**, *9*, 2282–2290.
[14] M. A. Sheik-Bahaei, A. Said, T. D. Wei, J. Hagan, E. W. Van Stryland, *IEEE J. Quantum Electron.* **1990**, *26*, 760–769.
[15] B. Sridevi, S. J. Narayan, A. Srinivasan, M. V. Reddy, T. K. Chandrashekar, *J. Porphyrins Phthalocyanines* **1998**, *2*, 69–78.
[16] a) E. Vogel, M. Bröring, J. Fink, D. Rosen, H. Schmickler, J. Lex, K. W. K. Chan, Y.-D. Wu, D. A. Plattner, *Angew. Chem. Int. Ed. Engl.* **1995**, *34*, 2511–2514; b) M. Bröring, J. Jendrny, L. Zander, H. Schmickler, J. Lex, Y.-D. Wu, M. Nendel, J. Chen, D. A. Plattner, K. N. Houk, E. Vogel, *Angew. Chem. Int. Ed. Engl.* **1995**, *34*, 2515–2517; c) G. R. Geier III, S. C. Grindrod, *J. Org. Chem.* **2004**, *69*, 6404–6412; d) H. Rath, J. Sankar, V. PrabhuRaja, T. K. Chandrashekar, B. S. Joshi, R. Roy, *Chem. Commun.* **2005**, 3343–3345.
[17] R. Kumar, R. Misra, T. K. Chandrashekar, E. Suresh, *Chem. Commun.* **2007**, 43–45.
[18] a) A. D. Becke, *J. Chem. Phys.* **1993**, *98*, 5648–5652; b) C. Lee, W. Yang, R. G. Parr, *Phys. Rev. B: Condens. Matter.* **1988**, *37*, 785–789.
[19] M. J. Frisch, G. W. Trucks, H. B. Schlegel, G. E. Scuseria, M. A. Robb, J. R. Cheeseman, J. A. J. Montgomery, T. Vreven, K. N. Kudin, J. C. Burant, J. M. Millam, S. S. Iyengar, J. Tomasi, V. Barone, B. Mennucci, M. Cossi, G. Scalmani, N. Rega, G. A. Petersson, H. Nakatsuji, M. Hada, M. Ehara, K. Toyota, R. Fukuda, J. Hasegawa, M. Ishida, T. Nakajima, Y. Honda, O. Kitao, H. Nakai, M. Klene, X. Li, J. E. Knox, H. P. Hratchian, J. B. Cross, V. Bakken, C. Adamo, J. Jaramillo, R. Gomperts, R. E. Stratmann, O. Yazyev, A. J. Austin, R. Cammi, C. Pomelli, J. W. Ochterski, P. Y. Ayala, K. Morokuma, G. A. Voth, P. Salvador, J. J. Dannenberg, V. G. Zakrzewski, S. Dapprich, A. D. Daniels, M. C. Strain, O. Farkas, D. K. Malick, A. D. Rabuck, K. Raghavachari, J. B. Foresman, J. V. Ortiz, Q. Cui, A. G. Baboul, S. Clifford, J. Cioslowski, B. B. Stefanov, G. Liu, A. Liashenko, P. Piskorz, I. Komaromi, R. L. Martin, D. J. Fox, T. Keith, M. A. Al-Laham, C. Y. Peng, A. Nanayakkara, M. Challacombe, P. M. W. Gill, B. Johnson, W. Chen, M. W. Wong, C. Gonzalez, J. A. Pople, *Gaussian 03*, Revision C.02 ed., Gaussian, Inc., Wallingford CT, **2004**.

Received: May 23, 2007
Published Online: July 17, 2007

